

# SparseLoc: Sparse Open-Set Landmark-based Global Localization for Autonomous Navigation

Pranjal Paul<sup>\*1</sup>, Vineeth Bhat<sup>\*1</sup>, Tejas Salian<sup>1</sup>, Mohammad Omama<sup>2</sup>,  
Krishna Murthy Jatavallabhula<sup>3</sup>, Naveen Arulselvan<sup>4</sup>, Madhava Krishna<sup>1</sup>

**Abstract**—Global localization is a critical problem in autonomous navigation, enabling precise positioning without reliance on GPS. Modern global localization techniques often depend on dense LiDAR maps, which, while precise, require extensive storage and computational resources. Recent approaches have explored alternative methods such as sparse maps and learned features, but they suffer from poor robustness and generalization. We propose *SparseLoc*<sup>1</sup>, a global localization framework that leverages vision-language foundation models to generate sparse, semantic-topometric maps in a zero-shot manner. It combines this map representation with a Monte Carlo localization scheme enhanced by a novel *late optimization* strategy, ensuring improved pose estimation. By constructing compact yet highly discriminative maps and refining localization through a carefully designed optimization schedule, *SparseLoc* overcomes the limitations of existing techniques, offering a more efficient and robust solution for global localization. Our system achieves over a 5× improvement in localization accuracy compared to existing sparse mapping techniques. Despite utilizing only 1/500<sup>th</sup> of the points of dense mapping methods, it achieves comparable performance, maintaining an average global localization error below 5m and 2° on KITTI.

## I. INTRODUCTION

Central to the advancement of autonomous driving systems is the mapping and localization task at the scale of a city. This involves modeling the surroundings sufficiently to estimate the navigating agent’s position within the map, enabling maneuvering throughout urban environments autonomously.

To achieve this, existing industry-led autonomous driving systems meticulously build dense representations of the environment, typically in the form of massive point cloud maps or high-definition maps containing lane-level information [1]. While these approaches provide centimeter-level precision, they impose memory and compute costs that become prohibitive when scaling beyond limited operational domains. Moreover, localizing in such maps generally requires a pose prior to globally estimate the agent’s position. Even sophisticated SLAM algorithms [2, 3] ultimately depend on tracking continuity or reliable initial pose estimates to recover from what is known as the “kidnapped robot problem”.

Attempting to address these challenges by compressing maps through heavy downsampling, but this merely represents a compromise that weakens accuracy due to the loss

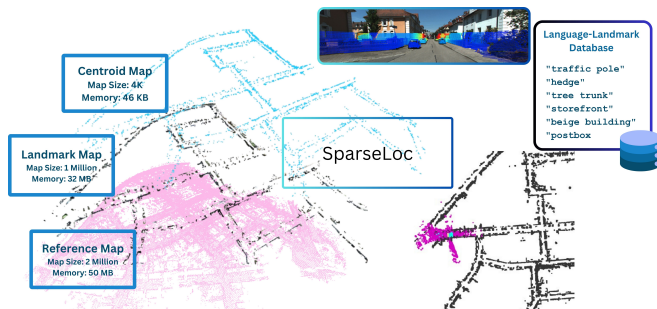


Fig. 1: *Introducing SparseLoc*. We introduce *SparseLoc*, a framework for constructing sparse, language-augmented object-centroid maps using open-set models, a robust data association scheme for accurate Monte Carlo global pose estimation, and a late optimization strategy to minimize localization errors.

of geometrical details inherent to the environment, without fundamentally addressing the scalability challenge.

Alternatively, oracle-based solutions like GNSS/GPS sensors or navigation maps such as OpenStreetMaps (OSM) are commonly employed [4]. These measurements of location using trilateration methods can become unreliable in urban environments due to multi-path effects and occlusions from skyscrapers.

Hence, it is desirable to build a map that is *representative* and can be consumed to perform self-localization - an ability to determine position within the mapped environment without any external assistance like GPS. The idea of a *representative map* follows from the observation that the majority of information in urban environments is concentrated in a small subset of structurally significant points. What truly matters for localization isn’t the raw quantity of points, but whether we have the *right points*. However, it can be difficult to simultaneously build a concentrated small subset of structurally significant points and also localize with sufficient precision.

Unlike mapping systems that process geometric features in metric space, humans navigate using cognitive spatial maps based on topological cues and distinctive environmental landmarks. While mapping systems see “just another building or trees” in metric coordinates, humans recognize “a blue building with adjacent rows of trees”. This distinction suggests potential benefits in integrating human-inspired localization principles into SLAM systems to distill environmental representations at the city scale; fundamentally, reimagining what constitutes a “map point”. Our study shows that rather than maintaining an elaborate set of points, we can sparsify the map by retaining a subset of points augmented

\* equal contribution

<sup>1</sup> Robotics Research Centre, IIT Hyderabad

<sup>2</sup> The University of Texas at Austin

<sup>3</sup> Facebook AI Research, Meta

<sup>4</sup> Ati Motors

<sup>1</sup>Project Page: <https://reachpranjal.github.io/sparseloc>

with foundational features to capture both geometric and semantic nuances. Essentially, we propose a concept of sparsity focusing on reducing the number of map points.

We introduce *SparseLoc*, a global localization framework that utilizes open-vocabulary perception models to construct compact, discriminative maps using landmark cluster centroids for sparse point representation which can be consumed by downstream localization and navigation modules. Our pipeline comprises of two key stages: an *Offline Sparse Map Construction* and an *Online Global Localization*, as illustrated in Fig. 2.

Our approach is validated through cross-dataset localization experiments between KITTI-360 Sequence 09 and KITTI-Raw Sequence 07, demonstrating robustness to viewpoint variations where traditional geometric methods generally fail, alongside standard global pose estimation experiments and navigation experiments.

Our contributions can be summarized as follows:

- 1) A framework using vision-language models to create semantically rich sparse maps that enable global localization. (Section III-A).
- 2) A Monte Carlo localization [5] technique with a novel *late optimization* approach showing faster convergence and reduced error. (Section III-B).
- 3) Empirical results showing improvement by 5 times over existing sparse-map techniques and comparable accuracy to dense-map methods at  $1/500^{th}$  the point density. (Table I, III).
- 4) Demonstrated robustness in cross-dataset scenarios with significant viewpoint variations. (Table IV).
- 5) System efficacy in CARLA simulation for navigation tasks, evaluated by goal reachability. (Section IV-D).

We *postulate* that combining classical methods with modern solutions offers the most promising path for autonomous navigation at the city scale, as demonstrated by *SparseLoc*'s integration of probabilistic localization with foundation models' semantic understanding capabilities.

## II. RELATED WORKS

**Global Localization Techniques on LiDAR Maps:** For global localization in LiDAR maps, most existing approaches [6–8] rely on geometric scan matching techniques or graph-theoretic approaches to align the current scan with a pre-registered LiDAR map. More recently, 3D-BBS [9] extended branch-and-bound-based 2D scan matching to 3D, achieving state-of-the-art results. However, all these approaches depend on dense LiDAR maps, which are computationally expensive and difficult to store and maintain at scale.

**Global Localization Techniques using Descriptors:** Methods under this category come in the form of place-recognition techniques where a scan descriptor is compared against a database of descriptors [10–12]. As they retrieve the scan but do not estimate the current pose, there is an additional layer that involves scan matching for pose refinement. Once again, it entails large storage requirements as maps increase in scale.

**Global Localization Techniques using Sparse Maps:** A number of approaches exist that have attempted to represent sparse maps in terms of specific landmarks such as poles [13], object-clusters [14], and OSM descriptors [15, 16]. We leverage object-level information through open-set models. Some fine registration techniques, such as That's My Point [17], operate on sparse points using estimates from global localization methods. Additionally, methods that perform fine localization given an initial estimate from an oracle [18] have been excluded from discussion, as they assume an external coarse localization source.

**Vision Language Models:** Vision-language models (VLMs) [19, 20] have achieved remarkable success across various domains, including open-set object detection [21] and segmentation [20]. Recent efforts have explored distilling VLM knowledge into 3D representations [22, 23], enabling the creation of open-vocabulary dense 3D maps for downstream tasks. Additionally, VLMs have demonstrated superior performance in vision-based place recognition [24].

Unlike prior works that rely on dense LiDAR scans or handcrafted sparse representations, we introduce a novel approach that utilizes open-world perception models to construct sparse, semantically-meaningful topometric maps for global localization. Our method eliminates the large memory requirement for dense map storage while achieving high localization accuracy, demonstrating the first zero-shot application of VLMs to sparse-map-based LiDAR localization at city-scale.

## III. METHODOLOGY

### A. Sparse Topometric Mapping

*SparseLoc* builds a lightweight language-augmented instance map of landmark centroids from posed RGB-LiDAR sequences. It uses off-the-shelf vision-language foundation models to identify static open-set landmarks, project the candidate instances to 3D metric space, and associate their cluster centroids across multiple views, constructing a highly sparse representation at kilometer scale that is consumed for the downstream task of localization.

**Open-Vocabulary Language-Landmark Database:** Our system uses pre-determined open-set labels for both mapping and localization runs. Assuming access to sufficient imagery data that covers the operating region<sup>2</sup>, we query the vision-language model  $\mathcal{V}(\cdot)$  over the entire image database to obtain a unique set of text-labels  $\mathcal{L} = \{l_q\}_{q=1}^Q$ . This reduces the likelihood of mis-detections that might otherwise occur in open-ended detection during localization. Moreover, by curating the database *a priori*, it establishes well-defined anchors – what counts as a landmark in the operating environment. We specifically instruct the model to focus on static objects suitable for localization while excluding dynamic elements such as vehicles and pedestrians. These

<sup>2</sup>While our approach requires image database which is typically available in common public datasets, in real-world application, it is a standard practice among existing industry-led autonomous driving systems to conduct initial mapping surveys before deployment.

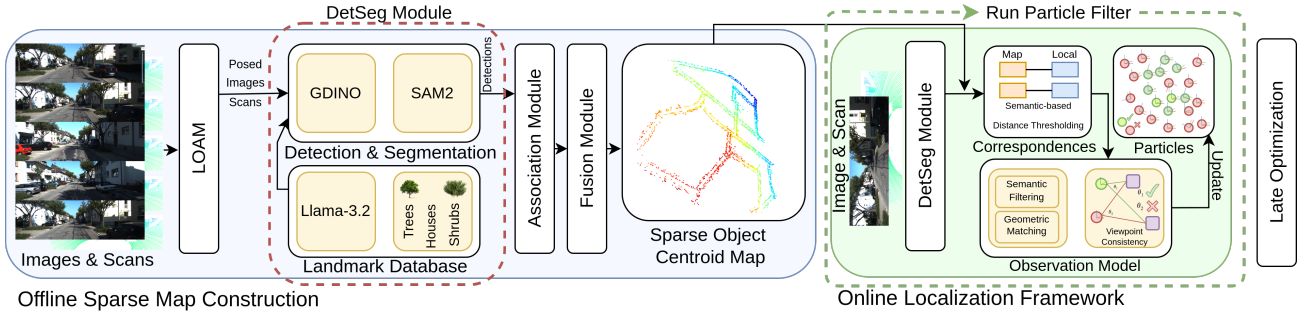


Fig. 2: *SparseLoc Architecture*. The framework consists of offline semantic-topometric sparse map construction and online global localization. The offline stage builds a compact landmark-based map using open-set models, while the online stage performs localization using Monte Carlo estimation and a novel Late Optimization to further refine our pose estimate.

descriptions serve as standardized textual identifiers for the landmarks throughout the pipeline.

### Landmark 2D Detection and Segmentation:

Given the language-landmark database and an input stream of calibrated RGB-LiDAR observations  $\mathcal{Z} = \{(\mathbf{I}_t^{rgb}, \mathbf{I}_t^{lidar}, \mathbf{U}_t)\}_{t=1}^T$  (Image, LiDAR Scan, Odometry) with ground-truth poses, we build a centroid map<sup>3</sup>  $\mathcal{M} = \{\mathbf{c}_k, l_k, \mathbf{f}_k\}_{k=1}^K$  where each point is characterized by the 3D position of the landmark cluster centroids  $\mathbf{c}_k$ , a language-aligned feature vector  $\mathbf{f}_k$  and the text-label  $l_k \in \mathcal{L}$  where  $K$  is the total number of *centroids* registered in the final constructed map  $\mathcal{M}$ .

We process each frame  $\mathbf{I}_t^{rgb}$  together with the landmark database  $\mathcal{L}$  through a grounding model  $\mathcal{G}(\cdot)$  to obtain precise 2D bounding boxes  $\mathbf{b}_t^{(i)}$  along with their semantic embedding<sup>4</sup>  $\mathbf{f}_t^{(i)}$  and a confidence score  $s_t^{(i)}$  directly obtained from the detection model:

$$(\mathbf{b}_t^{(i)}, \mathbf{f}_t^{(i)}, s_t^{(i)})_{i=1}^{N_t} = \mathcal{G}(\mathbf{I}_t^{rgb}, \{l_q\}_{q=1}^Q) \quad (1)$$

where  $N_t$  is the number of detected landmark instances at frame  $t$ . Further, when processing the calibrated input frame  $(\mathbf{I}_t^{rgb}, \mathbf{I}_t^{lidar})$ , we query a class-agnostic segmentation model  $\mathcal{S}(\cdot)$  for each detected region to obtain a pixel-level mask

$$\mathbf{m}_t^{(i)} = \mathcal{S}(\mathbf{I}_t^{rgb}, \mathbf{b}_t^{(i)}) \quad (2)$$

Each masked 2D instance is projected into 3D space using the calibration matrix, refined through DBSCAN clustering, and transformed to the map frame using the corresponding odometry pose  $\mathbf{U}_t$ . We then compute the centroid  $\mathbf{c}_t^{(i)}$  for each  $i^{th}$  cluster as the resultant instance observations  $\mathbf{o}_{t,i} = \langle \mathbf{c}_t^{(i)}, \mathbf{f}_t^{(i)}, l_t^{(i)} \rangle$ . Note that, for cases where the overlapping observations for different labels map to the same physical object, we tag the one with the highest confidence score  $s_t$  to the resulting cluster<sup>5</sup>. This ensures that each point in the map has a semantically accurate description.

<sup>3</sup>Our method can also be followed to distill landmarks from a pre-registered map containing aligned images, point-cloud scans and poses.

<sup>4</sup>Without loss of generality,  $\mathcal{G}(\cdot)$  can be followed by dedicated feature extractor  $\mathcal{E}(\cdot)$  to obtain semantic embedding  $\mathbf{f}_t^{(i)} = \mathcal{E}(\mathbf{b}_t^{(i)})$  parsing each detected regions.

<sup>5</sup>For the semantically similar observations, their feature vector can be also averaged out.

**Instance Association and Fusion:** Our association strategy mostly follows from [22] and has been overviewed in Fig. 2 as the association and fusion modules. As we detect new landmark instances  $\mathbf{o}_t^{(i)}$ , we evaluate their correspondence scores with all the existing instances  $\mathbf{o}_{t-1}^{(k)}$  registered so far in the map by computing: (1) the geometric similarity  $\phi_{geo}(i, k)$  which is the spatial proximity between instance clusters based on a nearest-neighbor ratio within a certain threshold, and (2) the semantic affinity measure  $\phi_{sem}(i, k)$ , a normalized cosine similarity between their feature vectors:  $\phi_{sem}(i, k) = \mathbf{f}_i^T \mathbf{f}_k / 2 + 1/2$ . The overall similarity score  $\phi(i, k)$  is the sum of both:  $\phi(i, k) = \phi_{sem}(i, k) + \phi_{geo}(i, k)$ . An instance association is established if  $\max_k \phi(i, k) > \delta_{sim}$ . In this case, we update the matched instance with the new observation by updating the point cloud, updating the feature vector through confidence-weighted averaging, and incrementing the observation count. If no suitable match is found, we initialize a new instance in the map.

### B. Multimodal Localization

Localization in large-scale environments presents significant challenges, particularly within the proposed framework due to: (1) the structural sparsity of the global map representation and (2) mean shifts in the landmark point cloud across scans, causing positional instability that prevents consistent 3D landmark correspondence. These factors hinder precise global alignment using a single scan. To address these challenges, we employ particle-filter-based localization, a recursive Bayesian state estimation method well-suited for incrementally refining pose estimates and achieving global convergence from multiple hypotheses as motion observations accumulate. However, robust data association is critical for consistent pose refinement, forming the core of our approach.

**Problem Setup:** Given a sequence of multimodal sensor observations  $\mathcal{Z}_t = \{(\mathbf{I}_t^{rgb}, \mathbf{I}_t^{lidar})\}_{t=1}^T$ , a relative odometry source  $\mathbf{U}_t = \{\mathbf{u}_t\}_{t=1}^T$  from some standard SLAM pipeline and our previously built semantically-augmented reference map  $\mathcal{M}$  together with language tags  $\mathcal{L}$ , we want to estimate a posterior distribution  $p(\mathbf{T}_t | \mathcal{Z}_{1:t}, \mathbf{U}_{1:t}, \mathcal{M}, \mathcal{L})$  of the robot's state  $\mathbf{T}_t \in SE(3)$  by approximating the distribution using  $N$  weighted pose hypotheses (particles)  $\{\mathbf{T}_t^{(i)}, w_t^{(i)}\}_{i=1}^N$  where

$w_t^{(i)}$  denotes the importance weight of the  $i^{th}$  particle:

$$w_t^{(i)} \propto p(\mathcal{Z}_t | \mathbf{T}_t^{(i)}, \mathcal{M}, \mathcal{L}) \cdot p(\mathbf{T}_t^{(i)} | \mathbf{T}_{t-1}^{(i)}, \mathbf{u}_t) \quad (3)$$

Our objective is to establish a multimodal observation likelihood function that returns optimal probabilistic correspondences between observed landmark centroids and the map landmarks.

**Prediction Step:** At initialization, we spawn  $N$  particles randomly across the map  $\mathcal{M}$ . Each particle  $\mathbf{T}_t^{(i)}$  is dead-reckoned using the relative odometry measurements, perturbed with Gaussian noise to account for odometry uncertainty. While this provides reasonable pose prior, it accumulates drift over time.

**Update Step:** To correct these accumulated errors, we define a refinement step that associates the observed landmark instances to the map context. Each incoming data is processed identically to the mapping phase to detect and segment open-set landmarks using equation (1) and equation (2) followed by extracting corresponding 3D point clusters. For each particle pose hypothesis  $\mathbf{T}_t^{(i)}$ , we compute the observation likelihood by comparing observed landmarks with map landmarks.

**Data Association and Weighting Mechanism:** We integrate both semantic and geometric landmark information for robust data association. Each particle represents a hypothesized robot pose, and if correct, the observed landmarks should align with mapped landmarks when transformed accordingly. This alignment is quantified by computing a weight contribution for each particle-landmark pair as follows:

- 1) **Semantic Filtering:** For each detected instance centroid  $\langle {}^{local}\mathbf{c}_t^{(j)}, \mathbf{f}_t^{(j)} \rangle$ , we first extract candidate map centroids using cosine similarity  $\phi_{sem}(j, k) > \delta_{sem}$  and transform them to particle’s frame  ${}^{local}\hat{\mathbf{c}}_k^{(i)} = \mathbf{T}_t^{(i)-1} \cdot {}^{map}\mathbf{c}_k$  where  $\mathbf{c}_k$  is the candidate centroid filtered from the map (abstracted as “*DetSeg*” module in Fig. 2).
- 2) **Geometric Matching:** The geometric compatibility is then computed based on the Euclidean distance between them and converted into a distance score using the exponential decay function:  $\phi_{dist}(j, k, i) = \exp\left(-\frac{e_d}{\alpha_{dist}}\right)$  where  $e_d = \|{}^{local}\hat{\mathbf{c}}_k^{(i)} - {}^{local}\mathbf{c}_t^{(j)}\|$  and  $\alpha_{dist}$  is a scaling parameter. This creates a soft matching score that decreases with distance.
- 3) **Viewpoint Consistency:** Euclidean distance alone is insufficient as it is viewpoint-agnostic; two points may be spatially close yet observed from different directions. A landmark observed at an angle  $\theta$  in the sensor frame should, under a correct pose hypothesis, appear at a similar angle in the particle frame. Viewing angle consistency is assessed by computing direction cosines relative to the observation frame axes and comparing them with the observed values in the hypothesized particle frame:

$$\phi_{angle}(j, k, i) = \frac{\cos(\Delta\theta) + 1}{2} \cdot \beta \quad (4)$$

where  $\Delta\theta$  is the absolute angular difference  $\arctan2(\cdot)$  between the landmark’s orientation in the observation frame and the candidate’s orientation in the particle frame and  $\beta = 1/(N \cdot \alpha)$  with scaling factor  $\alpha$  and total number of particles  $N$ .

- 4) **Overall Particle Weight:** Particle weights are updated exclusively based on current landmark observations, independent of prior weights. This enables the state estimator to adjust to new measurements rapidly without bias from past estimates. Each weight is determined by summing the highest-scoring landmark correspondences in the current frame.  $w_t^{(i)} \propto \sum_{j=1}^{N_L} \max_k \phi_{total}$  where  $\phi_{total}(j, k, i) = \phi_{sem} \cdot \phi_{dist} + \phi_{angle}$  which are then normalized using softmax with temperature  $\alpha_{softmax}$ .

**Resampling and Pose Estimation:** We periodically resample particles with replacement to concentrate in high-probability regions. The final pose estimate is then computed as the weighted average of all particle poses. For position components, we use standard weighted averaging:

$$\mathbf{t}_t = \sum_{i=1}^N w_t^{(i)\gamma} \cdot \mathbf{t}_t^{(i)} \quad (5)$$

where  $\gamma$  is a weight exponent parameter to control the influence of higher-weight particles. For rotation, we use circular averaging to properly handle the periodicity of the angular values.

$$\theta_t = \arctan 2 \left( \sum_{i=1}^N w_t^{(i)\gamma} \cdot \sin(\theta_t^{(i)}), \sum_{i=1}^N w_t^{(i)\gamma} \cdot \cos(\theta_t^{(i)}) \right) \quad (6)$$

where  $\theta_t$  is the axes angle resulting from the Rotation matrix computed from  $\phi_{i,j,k}$ . This prevents discontinuities that would occur with direct averaging of angles. For example, naively averaging  $359^\circ$  and  $1^\circ$  would yield  $180^\circ$ , while circular averaging correctly produces  $0^\circ$ , respecting the true shortest angular distance between the values.

**Late Optimization:** Once the particle filter converges to a coarse estimate, we perform pose refinement through a novel process that shares principles with pose-graph optimization. The key insight is to anchor the converged pose and retroactively improve the correspondences for previous observations within a history window  $\mathcal{H}$ , which will be leveraged to perform global optimization.

Given the converged particle pose  $\mathbf{T}_t$  at the current time  $t$ , we compute the refined pose for each previous timestamp  $t^- < t$ :  $\mathbf{T}_{t^-} = \mathbf{T}_t \times (\mathbf{T}_{t^- \rightarrow t}^{rel})^{-1}$  where  $\mathbf{T}_{t^- \rightarrow t}^{rel}$  represents the cumulative relative transformation from time  $t^-$  to  $t$  derived from odometry measurements. This relation can be expanded as the product of sequential relative transformations that were used in the predictive (dead-reckoning) steps:

$$\mathbf{T}_{t^- \rightarrow t}^{rel} = \mathbf{T}_{t^-+1}^{rel} \times \mathbf{T}_{t^-+2}^{rel} \times \dots \times \mathbf{T}_t^{rel} \quad (7)$$

Using these refined poses, we recompute landmark-to-

map correspondences<sup>6</sup> for each previous frame, resulting in correspondence sets  $\mathcal{C}_t$ , through a comprehensive matching process. This involves: (1) detecting landmark instances from sensor observations, (2) computing feature vectors for each detected instance, (3) matching these instances with candidate landmarks using cosine similarity of feature vectors, (4) filtering matches based on distance thresholds and positional constraints, and (5) constructing source-target centroid pairs for optimization.

We then perform a global optimization that considers  $\mathcal{C}_t$  to refine the particle pose.

$$\mathbf{T}^* = \arg \min_{\mathbf{T}} \sum_{i \in \mathcal{H}} \sum_{(j,k) \in \mathcal{C}_t} \|\mathbf{T} \cdot \mathbf{c}_j^{(i) \cdot local} - \mathbf{c}_k^{(i) \cdot map}\|^2 \quad (8)$$

where  $\mathbf{T}$  is the optimization variable. This global optimization finds a single transformation  $\mathbf{T}^*$  that best aligns all the previous landmarks observations in  $\mathcal{H}$  to the map structure.

### C. Implementation Details

*SparseLoc* is flexible to use any open-world detection and segmentation model, LLVM for landmark database and any odometry pipeline. For our experiments, we use Llama-3.2-Vision [19] for creating language-landmark database  $\mathcal{L}$ , Grounding-DINO [21] for detection and feature extraction  $\mathcal{G}(\cdot)$  and SAM2 [25] as segmentation model  $\mathcal{S}(\cdot)$ . We use variants of LOAM-family [2, 3] as back-end for odometry source as well as for creating the reference map and obtain aligned RGB-LiDAR scans.

In the mapping phase, we choose similarity score threshold to be  $\delta_{sim} = 0.7$  for instance association. A new instance is created if  $\phi_{sem}$  falls below this threshold. For localization, we initialize  $N = 1000$  particles randomly and uniformly distributed in the environment. In the data association step, we set the semantic similarity threshold to  $\delta_{sem} = 0.9$ , geometric matching scale factor  $\alpha_{dist} = 1$ , and viewpoint consistency coefficient  $\alpha = 10^{-3}$ . The temperature is set to  $\alpha_{softmax} = 0.5$  for normalized particle weight computation. For late optimization, we use a history window of  $\mathcal{H} = 10$  frames.

## IV. EXPERIMENTS

### A. Experimental Setup

We evaluate our approach using the KITTI dataset [26], focusing on sequences 00, 05, and 07. These sequences provide real-world urban environments suitable for our city-scale localization tasks. Table II details the characteristics of the corresponding sparse maps. Additionally, we perform cross-dataset validation by aligning segments of KITTI-09 from the KITTI-360 dataset [27] onto the sparse map constructed from KITTI-07.

<sup>6</sup>Direct ICP alignment was unstable due to sparse points and the requirement for hard correspondences. We evaluated two alternatives—RANSAC with the orthogonal Procrustes solution and an NLLS optimization over SE(3) with Huber loss—both yielding equivalent results.

Our evaluation consists of three key components: (1) benchmarking global localization performance against competing methods, (2) analyzing the impact of our late optimization strategy, and (3) demonstrating navigation capabilities using the generated sparse maps within the CARLA simulator.

### B. Global Localization Results

For benchmarking, compare our framework with both dense and sparse map-based localization methods [9, 15, 28].

**1) Comparison with Dense LiDAR Map-Based Localization:** We compare our approach against 3D-BBS [9] and KISS-Matcher [28]. 3D-BBS is a search-based localization method that directly estimates pose within the map, unlike descriptor-matching methods. 3D-BBS has positioned itself as a SOTA in global localization as its results seem to compare favorably with many popular methods like [7, 8]. KISS-Matcher is included for its novel global point cloud registration approach and state-of-the-art performance. We also adapt ROMAN [14] on KITTI but we get unreportable results with very high translation errors of 32 m on Sequence 00.

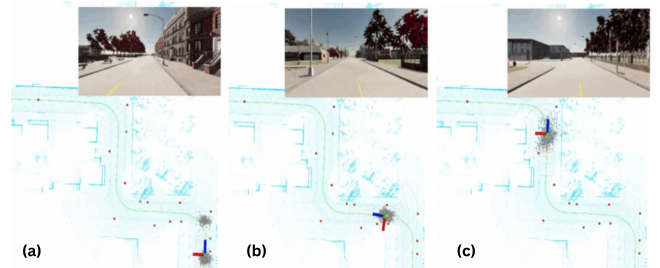


Fig. 3: *CARLA Navigation Runs*. Navigation run on CARLA demonstrating the efficacy of our sparse map. The red points are the mapped landmarks. The particle cloud is shown along with its mean as the reference converges from multi-modal to unimodal even around the first turn. Point-Cloud (in blue) is shown only for visualization.

Table I and III together reveal the strengths of our approach. Table I shows that we are better than KISS-Matcher at finer threshold while at a more relaxed threshold of 10 m, we surpass both the dense baselines. Notably, with nearly 500 times smaller map size, we achieve success rates of more than 99% for Sequences 00 and 05, and achieve 100% success rate for Sequence 07 at the relaxed threshold.

Table III shows that our sparse approach drastically outperforms KISS-Matcher in terms of average translation error (4.064m vs 107.0m for Sequence 00). This demonstrates that while our method may have slightly higher average errors, it is significantly more robust and consistent across different evaluation methodologies.

This performance difference stems from the fundamental nature of particle filters versus dense matching approaches. Dense methods achieve high precision when they successfully match features, but their lower success rates indicate they frequently fail to establish reliable correspondences, especially in urban environments with repetitive structures. Our particle filter approach maintains multiple localization

Method	Seq 00			Seq 05			Seq 07											
	(4m, 3°)		(10m, 5°)	(4m, 3°)		(10m, 5°)	(4m, 3°)		(10m, 5°)									
	$t_{avg}$	$r_{avg}$	$SR$															
KISS-Matcher [28]	<b>0.321</b>	1.382	33.54	<b>0.436</b>	1.912	42.41	<b>0.299</b>	1.166	44.57	<b>0.340</b>	<i>1.569</i>	53.26	<b>0.351</b>	1.043	77.42	<b>0.353</b>	1.140	80.65
3D-BBS [9]	<i>0.714</i>	<b>0.024</b>	<b>86.16</b>	<i>0.714</i>	<b>0.024</b>	<i>86.16</i>	<i>0.814</i>	<b>0.019</b>	<b>75.00</b>	<i>0.814</i>	<b>0.019</b>	<i>75.00</i>	0.759	<b>0.025</b>	<i>100.0</i>	0.759	<b>0.025</b>	<i>100.0</i>
<i>Ours</i>	2.103	<i>1.294</i>	<i>50.67</i>	4.054	<i>1.451</i>	<b>99.33</b>	1.293	<i>1.066</i>	<i>48.31</i>	3.150	<i>1.451</i>	<b>99.33</b>	<i>0.723</i>	<i>0.417</i>	<b>100.0</b>	<i>0.723</i>	<i>0.417</i>	<b>100.0</b>

TABLE I: *Quantitative comparison of global localization performance on KITTI sequences.* Reports the average translation error ( $t_{avg}$ , in meters), average rotation error ( $r_{avg}$ , in degrees), and success rate ( $SR$ , in percentage) at two different accuracy thresholds: (4m, 3°) and (10m, 5°). The best value for each metric is shown in **bold** font, while the second-best is *italicized*. Our method achieves the highest success rate in multiple cases, particularly at the (10m, 5°) threshold, while maintaining competitive accuracy compared to dense LiDAR-based approaches.

Seq.	Map Length (m)	LOAM Map Size	<i>Ours</i>
00	3,714	1,386,822	3,828
05	2,223	1,899,437	3,350
07	695	437,149	952

TABLE II: *Comparison of Map Size on KITTI.* We achieve significant results on global localization and navigation despite being almost 500× smaller.

hypotheses simultaneously, making it inherently robust to ambiguity, which explains our near-perfect success rates despite occasional larger average errors.

### 2) Comparison with Sparse Map-Based Localization:

Table III presents results against [15], using data from [18]. Our method achieves at least 4 times higher accuracy while localizing within 20-40 KITTI frames (equivalent to a 20m run), whereas their approach requires 500 KITTI frames. While maintaining a comparable map density (4.0K vs. 4.5K landmarks), our method achieves significantly lower translation errors - 4.064m vs. 20.00m in Sequence 00, 5.456m vs. 25.00m in Sequence 05, and most notably 0.723m vs. 25.00m in Sequence 07. This represents an average error reduction of approximately 80% while using slightly fewer map points, suggesting our landmark selection and representation approach captures significantly more valuable information.

Furthermore, our method provides comprehensive pose estimation by reporting both translation and rotation errors, whereas OSM-based method [15] fails to report rotation metrics. The consistency of our performance across diverse environments, particularly in Sequence 07, demonstrates the robustness of our approach in varied settings. These results position our sparse landmark-based method much closer to dense approaches in terms of accuracy while maintaining the efficiency advantages of sparse representation - using 250-500x fewer map points than dense methods like KISS-Matcher and 3D-BBS while achieving competitive localization performance.

3) *Cross-dataset Localization:* Cross-dataset localization presents a significant challenge, as localization is attempted across sequences captured at different times, often years apart. While these sequences may share substantial observation overlap, the set of sparse landmarks common to both becomes even sparser, exacerbating the difficulty of matching across substantial viewpoint and environmental variations. Our framework successfully localizes observations from KITTI-360’s 09 sequence within a sparse map

	Methods	Sparsity	Seq 00		Seq 05		Seq 07	
			$t_{avg}$	$r_{avg}$	$t_{avg}$	$r_{avg}$	$t_{avg}$	$r_{avg}$
Dense	KISS-Matcher [28]	2.1M	107.0	59.21	76.88	38.21	5.640	11.35
	3D-BBS [9]	1.0M	27.71	<b>0.335</b>	33.18	<b>0.503</b>	0.759	<b>0.025</b>
Sparse	OSM 4-bit des. [15]	4.5K	20.00	–	25.00	–	25.00	–
	<i>Ours</i>	4.0K	<b>4.064</b>	1.481	<b>5.456</b>	2.222	<b>0.723</b>	0.417

TABLE III: *Comparison of registration methods on KITTI sequences (Seq 00, Seq 05, Seq 07).* Reports the average translation error ( $t_{avg}$ , in meters) and average rotation error ( $r_{avg}$ , in degrees). We report approximate sparsity in terms of total map size (M for millions and K for thousands), only for Sequence 00.

generated from KITTI-360’s 07 sequence, despite the two sequences being captured approximately two years apart. This demonstrates the robustness of our approach to temporal and viewpoint changes. To quantitatively assess our localization accuracy, we perform coarse manual registration between sequences 09 and 07, allowing us to transform our estimated poses from 07’s frame to 09’s frame. Using this alignment, we evaluate the success rate of our localization, present in Table IV, reporting that greater than 80% success rates of observations from sequence 09 are localized within a 10m and 5° threshold on the sparse map from sequence 07.

Threshold	$t_{avg}$ (m)	$r_{avg}$ (°)	Success Rate (%)
4m, 3°	1.280	1.191	57.69
10m, 5°	2.065	1.672	80.77
15m, 7°	2.463	1.636	84.62

TABLE IV: *Cross-dataset Localization Results from KITTI-360 Sequence 09 on a Sparse Map from Sequence 07.* Reports the average translation error ( $t_{avg}$ , in meters), average rotation error ( $r_{avg}$ , in degrees), and success rate under three localization thresholds.

### C. Effect of the Late Optimization Schedule

Fig. 5 shows the impact of Late Optimization on translation error across three KITTI sequences (00, 05, and 07). The dropping arrows highlight the immediate error reduction after applying optimization: Sequence 00 shows a 0.79m (16.4%) reduction, Sequence 05 demonstrates a 1.12m (17.0%) decrease, and Sequence 07 exhibits the most significant improvement with a 1.02m (57.2%) reduction. These optimized estimates achieve accuracy comparable to what the particle filter would reach only after processing significantly more data, confirming that Late Optimization effectively refines localization results.

Notably, these refined estimates align with the accuracy achieved by the particle filter at 50m.

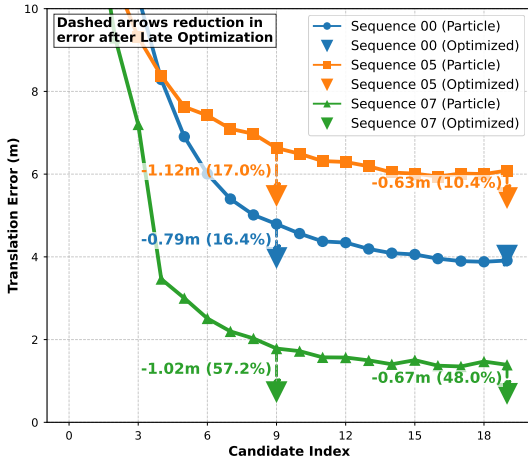


Fig. 4: *Impact of Late Optimization on KITT*. Late optimization reduces translation error by 30% at the 9th frame index (20 m) by refining the particle filter estimate, corresponding to our reported results. Also illustrated is optimization remains effective at the 19th frame but with diminishing returns.

#### D. Navigation with Sparse Maps

In this section, we demonstrate the effectiveness of our sparsely constructed semantically-augmented map for downstream navigation and goal-reaching tasks. Fig. 3 illustrates navigation runs on CARLA Town 01. The red points represent sparse landmark centroids registered onto the map and utilized during relocalization. We evaluate navigation performance based on goal reachability by measuring the distance between the vehicle’s final position and the goal location.

During navigation, the vehicle encounters viewpoint changes at turns and intersections that may cause perceptual aliasing. However, due to the multimodal nature of our particle filter approach, similar landmarks quickly disambiguate as the vehicle continues to move and converge faster to the correct location estimate. Across multiple autonomous navigation runs in Towns 01 and 02, we consistently achieved goal locations within a proximity of 2 meters as shown in Table V. These results further validate the efficacy of our sparse landmark-based approach for robust autonomous navigation in diverse urban scenarios.

Map Density	Map Length (m)	Town 01	Town 02
300 landmarks	1,500	1.55	1.63

TABLE V: *Closed-loop Navigation Performance*: Average goal reaching error (m) using our sparse landmark-based approach in CARLA Towns 01 and 02. Results demonstrate consistent sub-2-meter accuracy with minimal map density requirement (300 landmarks over 1,500m), validating the effectiveness of our particle filter-based relocalization method.

#### E. Role of Foundation Model and Sparsity Analysis

Foundation models, trained on web-scale data, excel at general semantic concepts. Our framework taps into the capabilities of such Open-World Perception models for localization through intuitive, zero-shot prompting to identify landmarks static to the scene. The VLM showed impressive

semantic understanding by automatically creating a landmark database, shown in Fig. 5, that was both sufficient and distinctive, working effectively across multiple KITT sequences without any changes. We only needed to prompt the VLM once for KITT Sequence 00, and this single database worked for all other sequences in our study. They were, however, filtered based on the grounding model’s detection capability. This perhaps marks the first significant use of VLMs specifically for localization and cross-localization across city-scale data. Further, the robustness of our approach is showcased by its effectiveness in cross-dataset localization scenarios which confront significant viewpoint and appearance variations, showcasing how foundational models can be effectively utilized for practical localization challenges.

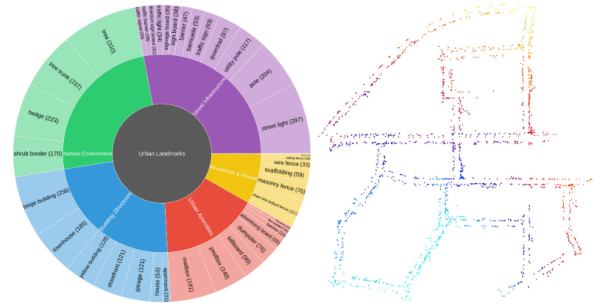


Fig. 5: *SparseLoc Database*. **Left**: shows the distribution of the landmarks registered. **Right**: Shows the registered landmark centroid map of KITT Sequence 00. They are sparse but reasonably distributed in urban scenes throughout the scale of the map. Image is best viewed at 5× zoom.

The inherent sparsity of our landmark-based mapping and localization approach introduces a challenge that as some landmarks appear with high frequency—such as trees, with new instances detected approximately every 5m (1.7 new detections per instance)—dominate over others (0.1–0.3 per instance). This uneven distribution leads to perceptual aliasing, continually testing the particle filter. Despite these challenges, our framework achieves strong localization accuracy by leveraging the multimodal hypothesis capabilities of particle filtering. Our work highlights the synergy between classical methods and modern AI, blending their strengths to create a robust, practical system for autonomous navigation.

## V. CONCLUSION

We presented *SparseLoc*, a global localization framework that leverages vision-language foundation models to generate sparse semantic-topometric maps in a zero-shot manner. By integrating a Monte Carlo localization scheme with a novel late optimization strategy, *SparseLoc* achieves robust and efficient pose estimation without the heavy computational and storage costs associated with dense LiDAR maps.

Experimental evaluations on urban datasets demonstrate that *SparseLoc* attains comparable global localization accuracy while using only a fraction of the points required by dense methods. These results validate the potential of our approach as a scalable and resource-friendly solution for autonomous navigation.

## REFERENCES

- [1] K. Wong, Y. Gu, and S. Kamijo, "Mapping for autonomous driving: Opportunities and challenges," *IEEE Intelligent Transportation Systems Magazine*, vol. 13, no. 1, pp. 91–106, 2020.
- [2] T. Shan and B. Englot, "Lego-loam: Lightweight and ground-optimized lidar odometry and mapping on variable terrain," in *IROS*, IEEE, 2018, pp. 4758–4765.
- [3] S. Yi, Y. Lyu, L. Hua, Q. Pan, and C. Zhao, "Light-loam: A lightweight lidar odometry and mapping based on graph-matching," *RAL*, 2024.
- [4] G. Floros, B. Van Der Zander, and B. Leibe, "Openstreetslam: Global vehicle localization using openstreetmaps," in *ICRA*, IEEE, 2013, pp. 1054–1059.
- [5] F. Dellaert, D. Fox, W. Burgard, and S. Thrun, "Monte carlo localization for mobile robots," in *ICRA*, IEEE, 1999.
- [6] H. Yin *et al.*, "A survey on global lidar localization: Challenges, advances and open problems," *International Journal of Computer Vision*, vol. 132, no. 8, pp. 3139–3171, 2024.
- [7] H. Yang, J. Shi, and L. Carlone, "Teaser: Fast and certifiable point cloud registration," *T-RO*, vol. 37, no. 2, pp. 314–333, 2020.
- [8] H. Lim *et al.*, "A single correspondence is enough: Robust global registration to avoid degeneracy in urban environments," in *ICRA*, IEEE, 2022, pp. 8010–8017.
- [9] K. Aoki, K. Koide, S. Oishi, M. Yokozuka, A. Banno, and J. Meguro, "3d-bbs: Global localization for 3d point cloud scan matching using branch-and-bound algorithm," in *ICRA*, IEEE, 2024, pp. 1796–1802.
- [10] J. Ma, J. Zhang, J. Xu, R. Ai, W. Gu, and X. Chen, "Overlaptransformer: An efficient and yaw-angle-invariant transformer network for lidar-based place recognition," *RAL*, vol. 7, no. 3, pp. 6958–6965, 2022.
- [11] R. Dubé, A. Cramariuc, D. Dugas, J. Nieto, R. Siegwart, and C. Cadena, "Segmap: 3d segment mapping using data-driven descriptors," *arXiv:1804.09557*, 2018.
- [12] M. A. Uy and G. H. Lee, "Pointnetvlad: Deep point cloud based retrieval for large-scale place recognition," in *CVPR*, IEEE, 2018, pp. 4470–4479.
- [13] A. Schaefer, D. Büscher, J. Vertens, L. Luft, and W. Burgard, "Long-term urban vehicle localization using pole landmarks extracted from 3-d lidar scans," in *ECMR*, IEEE, 2019, pp. 1–7.
- [14] M. B. Peterson, Y. X. Jia, Y. Tian, A. Thomas, and J. P. How, *Roman: Open-set object map alignment for robust view-invariant global localization*, 2024.
- [15] F. Yan, O. Vysotska, and C. Stachniss, "Global localization on openstreetmap using 4-bit semantic descriptors," in *ECMR*, IEEE, 2019, pp. 1–7.
- [16] Y. Cho, G. Kim, S. Lee, and J.-H. Ryu, "Openstreetmap-based lidar global localization in urban environment without a prior lidar map," *RAL*, vol. 7, no. 2, pp. 4999–5006, 2022.
- [17] G. Pramatarov, M. Gadd, P. Newman, and D. De Martini, "That's my point: Compact object-centric lidar pose estimation for large-scale outdoor localisation," in *ICRA*, IEEE, 2024, pp. 12 276–12 282.
- [18] M. Elhousni, Z. Zhang, and X. Huang, "Lidar-osm-based vehicle localization in gps-denied environments by using constrained particle filter," *Sensors*, vol. 22, no. 14, p. 5206, 2022.
- [19] H. Touvron *et al.*, "Llama: Open and efficient foundation language models," *arXiv:2302.13971*, 2023.
- [20] A. Radford *et al.*, "Learning transferable visual models from natural language supervision," in *ICML*, PmlR, 2021, pp. 8748–8763.
- [21] S. Liu *et al.*, "Grounding dino: Marrying dino with grounded pre-training for open-set object detection," in *ECCV*, Springer, 2024, pp. 38–55.
- [22] Q. Gu *et al.*, "Conceptgraphs: Open-vocabulary 3d scene graphs for perception and planning," *arXiv*, 2023.
- [23] K. M. Jatavallabhula *et al.*, "Conceptfusion: Open-set multimodal 3d mapping," *arXiv:2302.07241*, 2023.
- [24] M. Omama, P.-h. Li, and S. P. Chinchali, *Exploiting distribution constraints for scalable and efficient image retrieval*, 2024.
- [25] N. Ravi *et al.*, "Sam 2: Segment anything in images and videos," *arXiv:2408.00714*, 2024.
- [26] A. Geiger, P. Lenz, C. Stiller, and R. Urtasun, "Vision meets robotics: The kitti dataset," *The international journal of robotics research*, vol. 32, no. 11, pp. 1231–1237, 2013.
- [27] Y. Liao, J. Xie, and A. Geiger, "Kitti-360: A novel dataset and benchmarks for urban scene understanding in 2d and 3d," *TPAMI*, vol. 45, no. 3, pp. 3292–3310, 2022.
- [28] H. Lim *et al.*, "Kiss-matcher: Fast and robust point cloud registration revisited," *arXiv:2409.15615*, 2024.